Comprehensive Structure Analysis of Ordered Carbon Nanopipe Materials CMK-5 by X-ray Diffraction and Electron Microscopy

Leonid A. Solovyov,*,† Tae-Wan Kim,‡ Freddy Kleitz,‡ Osamu Terasaki,§ and Ryong Ryoo‡

Institute of Chemistry and Chemical Technology, 660049 Krasnoyarsk, Russia, National Creative Research Initiative Center for Functional Nanomaterials, Department of Chemistry (School of Molecular Science BK-21), Korea Advanced Institute of Science and Technology, Daejeon, 305-701, Republic of Korea, and Structural Chemistry, Arrhenius Laboratory, Stockholm University, S-106 91 Stockholm, Sweden

Received December 3, 2003

The structure of ordered mesoporous carbon materials CMK-5 was analyzed in detail by transmission electron microscopy (TEM) and X-ray diffraction (XRD) analysis by applying the recently developed continuous density function technique. The materials present two-dimensional (2-D) hexagonally ordered arrays of carbon nanopipes formed within the mesopores of SBA-15 silica templates used for their fabrication. The series of CMK-5 carbons were synthesized by applying the templates of different pore widths and two carbon precursors: furfuryl alcohol and acenaphthene. All the materials were well-ordered, exhibiting five distinct XRD reflections, high nitrogen BET specific surface areas (about 2500 m^2/g), and large pore volumes (about 2 cm^3/g). TEM analysis and XRD modeling allowed precise determination of the mesostructure characteristics such as the nanopipe diameter, wall thickness, and shape. Around 15% of the space between the nanopipes was found to be occupied by carbon interconnections formed inside the complementary pores of the SBA-15 templates. The structure parameters determined correlated well with the synthesis procedures and were fully consistent with the nitrogen adsorption and thermogravimetric data. The differences in the properties and the formation mechanisms of the materials synthesized by applying furfuryl alcohol and acenaphthene carbon precursors were analyzed based on the whole scope of data obtained.

1. Introduction

Porous carbons, owing to their surface properties and stability, are very attractive for applications in various areas, such as adsorption, purification of water, catalysis, electrochemistry, and others. Recently, the successful synthesis of mesostructured mesoporous carbons (MMCs) was discovered,[1,2] in which ordered mesoporous silicas were employed as templates. Compared to materials with disordered pore systems, MMCs allow precise control over their pore dimensions and arrangement, which is vital for applications requiring size and shape selectivity, hierarchical material organization, and pore accessibility. The use of ordered mesoporous templates permits obtaining carbons with high specific surface areas (ca. 2000 m^2/g) and pore volumes (ca. 1.5 cm^3/g). Due to high mesoscopic ordering, these materials offer a unique opportunity to study their structure by physical methods such as X-ray diffraction, electron microscopy, and physisorption.

The templated synthesis procedure applied in MMCs preparation allows a flexible tailoring of the material pore system by varying the synthesis conditions. The first MMCs were prepared in the form of an ordered array of carbon nanorods[3,4] or three-dimensional nanoframeworks[1,2,4,5] via complete filling of the template mesopores with carbon. Later, CMK-5 materials were presented,[6] which consisted of 2-D hexagonally ordered carbon nanopipes. Surface templating for these materials was achieved using SBA-15[7] templates in aluminosilicate form, with the pyrolysis of the polymerized furfuryl alcohol carbon precursor being performed at high temperature under vacuum. Ordered carbon nanopipe materials were subsequently synthesized through catalytic chemical vapor deposition using a cobalt-containing SBA-15 template and ethylene as a carbon precursor.[8] The high-temperature pyrolysis of the polymerized furfuryl alcohol was recently utilized in

* To whom correspondence should be addressed. E-mail: leosol@icct.ru. Tel: 7-3912-49-56-63. Fax: 7-3912-23-86-58.
† Institute of Chemistry and Chemical Technology.
‡ Korea Advanced Institute of Science and Technology.
§ Stockholm University.

(1) Ryoo, R.; Joo, S. H.; Jun, S. *J. Phys. Chem. B* **1999**, *103*, 7743.
(2) Lee, J.; Yoon, S.; Hyeon, T.; Oh, S. M.; Kim, K. B. *Chem. Commun.* **1999**, 2177.
(3) Jun, S.; Joo, S. H.; Ryoo, R.; Kruk, M.; Jaroniec, M.; Liu, Z.; Ohsuna, T.; Terasaki, O. *J. Am. Chem. Soc.* **2000**, *122*, 10712.
(4) Ryoo, R.; Joo, S. H.; Kruk, M.; Jaroniec, M. *Adv. Mater.* **2001**, *13*, 677.
(5) Ryoo, R.; Joo, S. H.; Jun, S.; Tsubakiyama, T.; Terasaki, O. *Stud. Surf. Sci. Catal.* [CD-ROM] **2001**, *135*.
(6) Joo, S. H.; Choi, S. J.; Oh, I.; Kwak, J.; Liu, Z.; Terasaki, O.; Ryoo, R. *Nature* **2001**, *412*, 169.
(7) Zhao, D.; Huo, Q.; Feng, J.; Chmelka, B. F.; Stucky, G. D. *J. Am. Chem. Soc.* **1998**, *120*, 6024.

10.1021/cm0352652 CCC: $27.50
Published on Web 04/24/2004

preparing tubular MMCs with cubic *Ia*3*d* symmetry.[9,10] MMCs with adjustable nanopipe diameter and wall thickness were obtained using mesoporous templates of different pore widths and two-step procedure of carbon precursor infiltration.[11] Recently, MMCs with bimodal pore size distributions were reported, which were prepared utilizing diluted furfuryl alcohol carbon precursor.[12]

Nanopipe MMCs were characterized by applying different physical and chemical methods,[11−13] but many important questions concerning their structure and its relation to the formation mechanism have remained unanswered. Estimations of the internal and external carbon nanopipe diameters for different CMK-5 materials were done on the basis of a combined nitrogen adsorption analysis of the carbons, the silica/carbon composites, and the SBA-15 templates.[11,13] However, only the range 0.6−1.3 nm was determined for the nanopipe wall thickness[11] since the uncertainty in the nanopipe diameter estimations did not permit deriving definite values for definite samples. Another important characteristic of MMCs prepared using SBA-15 and other block-copolymer-templated mesoporous silicas, which has not been determined by adsorption analysis, is the interconnectivity of MMC building elements. The success of MMC synthesis using SBA-15 template was based on its complementary porosity that provides connections between the adjacent mesopore channels and, consequently, prevents the resulted carbon material from collapse.[3] The degree of interconnectivity determines important functional properties of MMCs, such as mechanical strength and stability. In addition, its value may be used as an estimate of the complementary porosity of the parent template itself.

Obvious difficulties in structure analysis of MMCs and other mesostructured materials are due to their disordering at the atomic level, which hinders applications of well-developed standard crystallographic approaches. XRD and TEM have been applied so far to CMK-5 materials only for measuring their 2-D hexagonal lattice parameters and for qualitative structure description. In the present work a detailed TEM and XRD structure analysis of a series of CMK-5 materials is performed by applying the recently developed continuous density function (CDF)[14,15] technique. The internal and external diameters of the carbon nanopipes, their wall thickness, and the density of interconnections are determined for CMK-5 samples prepared using SBA-15 templates with different pore widths. The structural parameters obtained are discussed in correlation with the synthesis procedures based on two carbon precursors: furfulyl alcohol and acenaphthene. The use of the latter was recently shown to provide mesostructured carbons with improved mechanical stability and higher graphitization.[16] In this respect, it was interesting to compare the structure characteristics of carbons prepared from these two precursors. The density distribution maps obtained from TEM and XRD modeling are described, and conclusions about the distribution of interconnections between the carbon nanopipes are made.

2. Materials and Methods

2.1. Materials. Three samples of SBA-15 silica with different pore diameters were prepared using surfactants of different sizes or surfactant mixtures.[11] These silica samples are denoted by Silica-L, -M, and -S (L, M, and S standing for "large pore", "medium pore", and "small pore", respectively). The details of the synthesis procedures are as follows: Silica-L was synthesized using tetraethyl orthosilicate (TEOS) and the $EO_{20}PO_{70}EO_{20}$ surfactant (Pluronic P123 of Aldrich) following the SBA-15 synthesis procedure reported previously.[3,7] Four grams of P123 was dissolved in 150 g of 1.6 M HCl solution at 308 K; 8.50 g of TEOS was added with vigorous stirring. After being stirred for 15 min, the mixture was kept under static conditions in an oven at the same temperature for 24 h. Subsequently, the mixture containing the precipitated product was heated at 373 K for 24 h. Silica-M was synthesized in the same way as Silica-L, except for the use of sodium silicate solution (1.3 wt % Na_2O, 5.0 wt % SiO_2, and 93.7 wt % H_2O) and the $EO_{17}PO_{60}EO_{17}$ surfactant (Pluronic P103, BASF). That is, 49.6 g of the sodium silicate solution was added to the solution of 4 g of P103 dissolved in 104.2 g of 1.6 M HCl at 308 K. The remainder of the synthesis procedure was the same as for Silica-L. The synthesis of Silica-S was carried out with a surfactant mixture consisting of 2.8 g of P103, 0.6 g of the $C_{12}EO_7$ surfactant [$C_{12}H_{25}O(C_2H_5O)_7H$, Hannong LE-7], and 0.6 g of $C_{12}EO_5$ (Hannong LE-5), which were dissolved in 105.2 g of 0.86 M HCl solution. To this solution 44.8 g of sodium silicate solution was added at 308 K with stirring. Stirring was continued for 12 h at the same temperature. Then, the resultant mixture was aged at 373 K for 12 h under static conditions.

All silica products were filtered without washing, dried at 373 K, washed with ethanol, and calcined at 673 K. The calcined silica samples were impregnated with aqueous solution of $AlCl_3$ (typically, Si/Al = 20).[17,18] After the solvent water was completely evaporated in a rotary evaporator, the samples were calcined in air at 823 K. The Al incorporation was carried out to donate the mesopore walls an acid catalytic activity for the carbonization of furfuryl alcohol and acenaphthene.

Silica-L was used for carbon synthesis as calcined or after silylation, to modify the surface in a hydrophobic way. All other silica samples were used as calcined. The silylation of Silica-L was performed following the procedure described elsewhere.[19] Briefly, 1 g of Silica-L sample and 10 mL of toluene were placed in a round-bottom flask. Subsequently, 2.09 mL of trimethylchlorosilane (98%, Aldrich) was added and the mixture was refluxed at 423 K for 1 d. After the mixture was cooled to room temperature, the product was filtered with ethanol washing and dried at 373 K in an oven. This sample was denoted by Silica-L−S.

Sample CMK-5-LG (LG standing for "large pore and graphitic") was synthesized using Silica-L−S as a template and acenaphthene as a carbon precursor. 1 g of Silica-L−S and 1.03 g of acenaphthene (99%, Aldrich) were put into vacuum-

(8) Zhang, W.-H.; Liang, C.; Sun, H.; Shen, Z.; Guan, Y.; Ying, P.; Li, C. *Adv. Mater.* **2002**, *14*, 1776.
(9) Kleitz, F.; Choi, S. H.; Ryoo, R. *Chem. Commun.* **2003**, 2136.
(10) Che, S.; Garcia-Bennett, A. E.; Liu, X.; Hodgkins, R. P.; Wright, P. A.; Zhao, D.; Terasaki, O.; Tatsumi T. *Angew. Chem., Int. Ed.* **2003**, *42*, 3930.
(11) Kruk, M.; Jaroniec, M.; Kim, T.-W.; Ryoo, R. *Chem. Mater.* **2003**, *15*, 2815.
(12) Lu, A. H.; Schmidt, W.; Spliethoff, B.; Schuth, F. *Adv. Mater.* **2003**, *15*, 1602.
(13) Darmstadt, H.; Roy, C.; Kaliaguine, S.; Kim, T.-W.; Ryoo, R. *Chem. Mater.* **2003**, *15*, 3300.
(14) Solovyov, L. A.; Kirik, S. D.; Shmakov, A. N.; Romannikov V. N. *Microporous Mesoporous Mater.* **2001**, *44-45*, 17.
(15) Solovyov, L. A.; Belousov, O. V.; Shmakov, A. N.; Zaikovskii, V. I.; Joo, S. H.; Ryoo, R.; Haddad, E.; Gedeon, A.; Kirik, S. D. *Stud. Surf. Sci. Catal.* **2003**, *146*, 299.
(16) Kim, T.-W.; Park, I.-S.; Ryoo, R. *Angew. Chem., Int. Ed.* **2003**, *42*, 4375.
(17) Jun, S.; Ryoo, R. *J. Catal.* **2000**, *195*, 237.
(18) Ryoo, R.; Jun, S.; Kim, J. M.; Kim, M. J. *Chem. Commun.* **1997**, 2225.
(19) Jaroniec, M.; Jaroniec, C. P.; Kruk, M.; Ryoo, R. *Adsorption* **1999**, *5*, 313.

sealed Pyrex tubing. The tubing was heated to 523 K over 3 h and then maintained at 523 K for 6 h in a furnace. The product was collected after the tubing was cooled to room temperature. The product was heated at 1173 K for 11 h under vacuum in a fused quartz reactor. The resultant carbon/silica composite and the carbon sample were denoted Composite-LG and CMK-5-LG, respectively.

Three kinds of CMK-5-X samples (X = L, M, and S) were prepared following the same procedures described elsewhere.[6,11,13] The pores of Silica-L, -M, and -S were filled with furfuryl alcohol by incipient wetness at room temperature. The furfuryl alcohol/SBA-15 composites were heated overnight at 368 K in a closed bottle for polymerization. The polymerized alcohol was converted to carbon at 1173 K under vacuum. The carbon−silica composites thus obtained were denoted Composite-L, -M, and -S. Finally, the template was removed with HF solution. The resultant carbon samples were denoted CMK-5-L, -M, and -S.

2.2. Methods. XRD data were collected on a laboratory powder diffractometer (DRON-4, Cu Kα radiation) with a primary beam collimator and a secondary flat graphite monochromator. The measurements were performed in Bragg−Brentano geometry. The primary beam was collimated by two slits of 0.1 mm displaced at 60 mm from each other. XRD structure modeling was performed using the CDF technique.[14,15] The internal structure disorder was allowed for by incorporating the Debye−Waller factor. The Rietveld's full-profile formalism[20] was applied in the XRD powder profile calculations. The calculations were carried out using a computer code package based on a corrected and modified version of the Rietveld refinement program DBWS-9006PC.[21]

TEM images were taken by a JEOL JEM-4000EX instrument operated at 400 kV.

Nitrogen adsorption−desorption isotherms were measured at 77 K on a Quantachrome Autosorb-1MP volumetric adsorption analyzer. Before the adsorption measurements, samples were outgassed at 573 K in the port of the adsorption analyzer. The values of carbon-to-silica ratio in the composite samples were measured by a TA Instruments TGA 2050 thermogravimetric analyzer. The heating rate was 5 K/min in air.

3. Results and Discussion

XRD powder patterns of the CMK-5 samples studied are shown in Figure 1. All the materials exhibit five distinct nonzero diffraction peaks, indicating their high ordering. XRD patterns of CMK-5 carbons differ noticeably from those of CMK-3, which is known to consist of carbon nanorods.[3,25] The most marked difference is the inverse ratio between the intensities of reflections 10 and 11. This difference in XRD patterns of CMK-5 and CMK-3 is, evidently, related to the internal structure of these materials. The initial model of CMK-5 structure can be derived from transmission electron microscopy. A TEM image of sample CMK-5-L viewed along the carbon nanopipe axis is shown in Figure 2a. TEM allows qualitative characterization of the material as a two-dimensional hexagonal array of carbon nanopipes as was already reported earlier.[6]

To build the initial model of averaged density distribution in CMK-5, we used a technique of density reconstruction that has been successfully applied in the analysis of mesostructured substances by electron microscopy.[22,23] The modules and phases of the crystal structure factors were extracted from the Fourier transforms of selected regions of TEM images. No correction

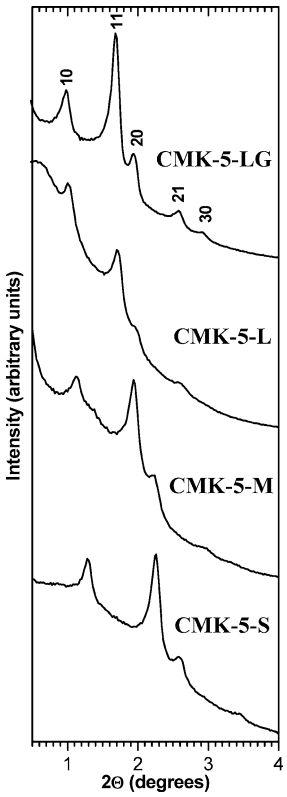

Figure 1. XRD powder patterns of the CMK-5 carbons studied.

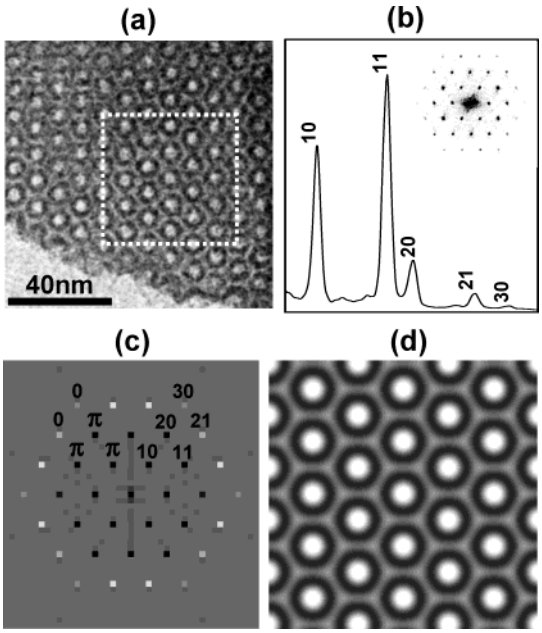

Figure 2. (a) TEM image of CMK-5-L taken along the nanopipe axis. (b) Fourier diffractogram of the TEM image and the profile of its rotational averaging. (c) The real part of the Fourier transform of the TEM image averaged for a series of fragments. The dark, gray, and bright levels correspond to negative, nearly zero, and positive values, respectively. The reflection indexes (10, 11, 20, 21, 30) and phases (π, π, π, 0, 0) are labeled. (d) Density reconstruction based on the structure factor modules and phases extracted from the Fourier transforms of the TEM image.

(20) Rietveld, H. M. *J. Appl. Crystallogr.* **1969**, *2*, 65.
(21) Wiles, D. B.; Young, R. A. *J. Appl. Crystallogr.* **1981**, *14*, 149.
(22) Carlsson, A.; Kaneda, M.; Sakamoto, Y.; Terasaki, O.; Ryoo, R.; Joo, S. H. *J. Electron Microsc.* **1999**, *48*, 795.
(23) Sakamoto, Y.; Kaneda, M.; Terasaki, O.; Zhao, D. Y.; Kim, J. M.; Stucky, G.; Shin, H. J.; Ryoo, R. *Nature* **2000**, *408*, 449.
(24) Le Bail, A.; Duroy, H.; Fourquet, J. L. *Mater. Res. Bull.* **1988**, *23*, 447.
(25) Solovyov, L. A.; Shmakov, A. N.; Zaikovskii, V. I.; Joo, S. H.; Ryoo, R. *Carbon* **2002**, *40*, 2477.

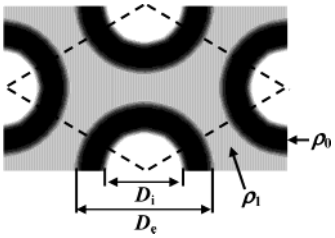

Figure 3. Model of density distribution in CMK-5. The two-dimensional lattice unit cell is outlined by dashed lines.

was done for the contrast transfer function (CTF) since at this stage we were aimed only at qualitative characterization of the initial structure model. Besides, the focusing conditions used guaranteed no change of CTF signs in the region of wavenumbers <0.4 nm^{-1} where all the diffraction peaks of interest were observed. Figure 2b shows a typical Fourier diffractogram and the profile of its rotational averaging for the TEM image of CMK-5. As can be seen, the rotational averaging profile demonstrates good consistency in the diffraction peak intensities between the Fourier diffractogram and the XRD powder patterns (Figure 1), which indicates that the TEM image region used is representative of the bulk material. In Figure 2c the real part of the TEM image Fourier transform is mapped. Since the material symmetry (*p*6*mm*) includes the inversion center, the structure factor phases may be reduced to only two values: either 0 or π. In this case the phases can be determined from the signs of the real part of peaks in the TEM image Fourier transforms provided the origin and size of the Fourier-transformed regions are properly chosen. The Fourier transform picture shown in Figure 2c was typical of all the representative TEM regions and allowed unambiguous determination of the structure factor phases. For proper averaging the structure factor modules were determined from the Fourier diffractogram (shown in Figure 2b) of a big representative TEM image fragment.

In Figure 2d, the density distribution map for CMK-5 is shown, calculated on the basis of the structure factor modules and phases extracted from the TEM image by the described above procedure. The map shows that the rings corresponding to the carbon nanopipe projections are basically circular (not hexagonal) by shape and the averaged density distribution between the nanopipes is approximately uniform. On the basis of the TEM analysis, the model of density distribution in CMK-5 was chosen as shown in Figure 3. The circular ring areas of higher density ρ_0 related to the carbon nanopipes with internal and external diameters D_i and D_e respectively are separated by a region of lower constant density ρ_1 representing the interconnections between the nanopipes. The density inside the nanopipes is assumed to be zero.

The variable structure parameters D_i and D_e, and the ratio ρ_1/ρ_0 were determined for the series of CMK-5 carbon samples from powder XRD profile modeling by applying the CDF technique. In parallel, XRD modeling was also performed for the silica/carbon composites and for the SBA-15 templates recovered from the composites after carbon combustion (4 h at 873 K). Preliminary structure refinement revealed certain correlations between the Debye−Waller factor and the structure parameters of the carbon samples. To overcome this problem, several structure modeling runs were carried out by applying a sequence of fixed Debye−Waller factors. Among these modeling runs the most successful were chosen, which allowed the best consistency between the diameters D_e and D_i determined for all three types of samples: the CMK-5 carbons, the respective silica/carbon composites, and the recovered SBA-15 templates. The deviations in D_e and D_i between the three types of samples were within 0.15 nm, which can be used as an estimate of the XRD modeling accuracy. The final fit between the experimental and calculated XRD profiles obtained by structure modeling is shown in Figure 4. As seen, the refined structure model allowed

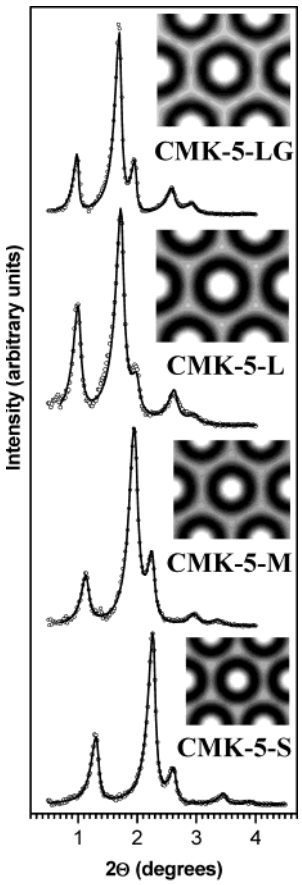

Figure 4. Experimental (circles) and calculated (solid line) X-ray powder diffraction profiles for the CMK-5 carbon samples. The background line is subtracted for better representation. The insets show the respective density distribution maps.

Table 1. Structural Characteristics of the CMK-5 Carbons Determined from XRD Modeling and Physisorption[a]

sample	*a* (nm)	D_i (nm)	D_e (nm)	*t* (nm)	ρ_1/ρ_0	*u* (nm)	S_{BET} (m^2/g)	V_t (cm^3/g)
CMK-5-LG	10.51	5.8	8.0	1.1	0.15	0.45	1827	1.465
CMK-5-L	10.35	5.9	7.9	1.0	0.14	0.62	2098	1.966
CMK-5-M	9.15	4.9	6.6	0.9	0.17	0.61	2693	2.117
CMK-5-S	7.79	4.4	5.8	0.7	0.13	0.66	2480	1.954

[a] *a*, the unit cell parameter; D_i and D_e, the internal and external diameters of the carbon nanopipes; ρ_0, the scattering density of the nanopipe wall; ρ_1, the average scattering density of the material in the region between the nanopipes; *t*, the thickness of the nanopipe walls given by $(D_e - D_i)/2$; *u*, the mean amplitude of displacement (disordering) of the structure elements derived from the Debye−Waller factor; S_{BET}, the BET specific surface area deduced from the isotherm analysis in the relative pressure range from 0.05 to 0.20; V_t, the total pore volume at relative pressure 0.95.

Table 2. Observed (F_{obs}) and Calculated (F_{clc}) Structure Factor Modules and Phases for the CMK-5 Samples Obtained from XRD Modeling[a]

reflection indexes	CMK-5-LG		CMK-5-L		CMK-5-M		CMK-5-S		phases[b]
	$\|F_{obs}\|$	$\|F_{clc}\|$	$\|F_{obs}\|$	$\|F_{clc}\|$	$\|F_{obs}\|$	$\|F_{clc}\|$	$\|F_{obs}\|$	$\|F_{clc}\|$	
10	31.72	31.57	45.87	46.18	36.15	36.45	38.38	38.31	π
11	100.0	100.29	100.0	99.73	100.0	99.92	100.0	99.89	π
20	58.40	58.25	46.00	45.63	55.71	55.08	46.49	48.18	π
21	32.05	31.42	35.10	34.61	25.69	24.99	23.40	23.20	0
30	33.88	33.92	26.84	25.79	23.60	24.63	16.25	18.98	0
R_F:	0.5%		1.0%		1.1%		2.1%		

[a] R_F, the reliability factor characterizing the overall percent difference between the observed and calculated structure factor modules. [b] The same sequence of the structure factor phases was obtained for all the samples.

perfect agreement between the experimental and calculated XRD profiles. The structural characteristics of CMK-5 samples are summarized in Table 1. The observed and calculated structure factors are presented in Table 2. The observed structure factor modules were derived from the powder XRD profiles by applying the Le Bail algorithm.[24]

To reveal additional structure details which might be omitted by the simplified model used, we performed calculations of the density distribution maps based on the structure factor modules determined from the XRD profiles and the phases derived from the refined structure model (Table 2). The density distribution maps shown in Figure 4 did not demonstrate additional features that could be related to new structure details except local maxima in the region between the nanopipes. Similar maxima were also observed for CMK-3 materials and related to the carbon interconnections.[25] These features might have been interpreted as a nonuniformity of the interconnection distribution between the nanopipes; however, the analysis of the difference density maps (based on the difference between the observed and calculated structure factors) did not reveal any appreciable maxima in the respective areas. From this we may conclude that the interconnections between the carbon nanopipes are distributed rather randomly and the local maxima observed in the density maps are related most probably to the overlapping of the averaged density distribution rings dispersed due to the local disordering of the nanopipes. Density distribution analysis also did not reveal regular deviations of the nanopipe shape from pure cylindrical, and the inclusion of the nanopipe hexagonality parameter into the structure model did not result in any improvement of the XRD profile fit.

The nitrogen adsorption isotherms and the pore size distributions (PSDs) for the CMK-5 carbons studied are shown in Figure 5. The PSDs demonstrate two overlapped peaks related to the two systems of mesopores bounded by the internal and the external cylindrical surfaces of the carbon nanopipes. The PSD maxima are better resolved for samples LG and L, for which the difference between the internal nanopipe diameters and the inter-nanopipe distances (related to the silica template wall thickness) is the biggest compared to the remaining samples.

The structure parameters of the SBA-15 templates and the silica/carbon composites are summarized in Table 3. As seen, the values of the carbon nanopipe diameters and wall thickness determined for the CMK-5 samples by XRD modeling (Table 1) correlate well with the structure parameters of the respective SBA-15

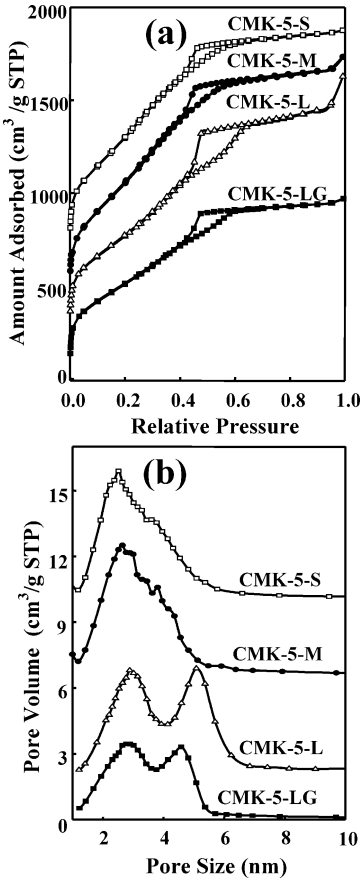

Figure 5. (a) Nitrogen adsorption−desorption isotherms for the CMK-5 carbon samples. The isotherms for samples L, M, and S are offset vertically by 200, 300, and 600 cm^3/g STP, respectively. (b) Pore size distributions (PSDs) calculated from the nitrogen adsorption isotherms for the CMK-5 carbon samples by the BJH method. The PSDs for samples L, M, and S were offset vertically by 2, 6.5, and 10 cm^3/g STP, respectively.

templates. The external and internal diameters of the nanopipes determined from XRD exceed the respective pore diameters of SBA-15 templates and silica/carbon composites determined from nitrogen adsorption data using the BJH[26] methods, which can be related to the well-known fact that the BJH analysis usually underestimates the width of mesopores.[27,28] Much better consistency between XRD- and adsorption-based pore diameters was obtained by applying the KJS[29] ap-

(26) Barrett, E. P.; Joyner, L. G.; Halenda, P. P. *J. Am. Chem. Soc.* **1951**, *73*, 373.
(27) Kruk, M.; Jaroniec, M.; Ryoo, R.; Joo, S. H. *Chem. Mater.* **2000**, *12*, 1414.
(28) Ravikovitch, P. I.; Neimark, A. V. *J. Phys. Chem. B* **2001**, *105*, 6817.

Table 3. Characteristics of the SBA-15 Templates and the Respective Silica/Carbon Composites[a]

	SBA-15 templates						silica/carbon composites		
sample	a (nm)	S_{BET} (m^2/g)	V_t (cm^3/g)	w_{BJH} (nm)	w_{KJS} (nm)	w_{XRD} (nm)	a (nm)	w_{BJH} (nm)	C (wt %)
CMK-5-LG[b]	11.12	539	0.749	6.7	7.4	7.7	10.55	4.9	25
CMK-5-L	11.81	676	0.906	7.5	8.2	8.4	10.60	5.0	31
CMK-5-M	9.61	693	0.858	6.3	7.0	7.0	9.18	3.9	35
CMK-5-S	8.39	813	0.854	4.8	5.5	6.3	7.80	3.6	32

[a] a, the unit cell parameter; S_{BET}, the BET specific surface area; V_t, the total pore volume; w_{BJH} and w_{KJS}, the pore diameters determined from the nitrogen adsorption data using the BJH[26] and the KJS[29] methods; C, the wt % of carbon determined by TGA. [b] The parameters of the silylated template are presented for sample CMK-5-LG.

proach. It must be noted that both the carbon nanopipe diameters and the wall thickness decrease with decreasing the lattice parameters and pore widths of the templates.

The idealized expected thickness of the carbon nanopipe walls in CMK-5 can be estimated from volumetric considerations taking into account the synthesis procedure. The nanopipe walls are formed of carbon from a precursor substance that fills the entire mesopore volume of SBA-15 template by the incipient wetness procedure. Therefore, assuming no carbon loss, the ratio of the cylindrical mesopore volume V_m to the expected volume occupied by carbon walls V_c can be given by the following equation,

$$\frac{V_m}{V_c} = \frac{D_m^2}{D_e^2 - D_i^2} = \frac{\rho_c}{W_c \rho_p} \quad (1)$$

where D_m is the template mesopore diameter, D_e and D_i are the external and internal diameters of the carbon nanopipes, ρ_c and ρ_p are the absolute densities of amorphous carbon (~2 g/cm^3)[30] and the carbon precursor, and W_c is the weight fraction of carbon in the precursor substance. Taking into account that diameters D_m and D_e do not differ much, we can derive the expected nanopipe wall thickness from eq 1 as

$$t_{exp} = (D_e - D_i)/2 \approx (D_m - D_i)/2 = D_m[1 - (1 - W_c\rho_p/\rho_c)^{1/2}]/2 \quad (2)$$

If we use w_{XRD} given in Table 3 as an approximation of the template mesopore diameters D_m for carbons synthesized using furfuryl alcohol precursor (W_c = 0.588, ρ_p = 1.135 g/cm^3), then the expected nanopipe wall thickness values for these samples (L, M, and S) may be evaluated from eq 2 as 0.77, 0.64, and 0.59 nm, respectively. The XRD modeling gave somewhat bigger nanopipe wall thickness values (see Table 1) than the expected ones, which can be explained by the fact that the nanopipe walls are not ideal. Kruk et al.[11] recently studied CMK-5 carbons similar to samples L, M, and S by nitrogen adsorption. They estimated the wall thickness of carbon nanopipes to fall within the interval 0.6–1.3 nm. They also showed that the carbon film introduced on the template surface was likely to be rough and microporous to some extent. Roughness and microporosity make the effective averaged density of the carbon nanopipe walls lower than the absolute density of amorphous carbon. Under the effective density of carbon nanopipe walls here we assume the ratio of the wall mass to the volume bounded by its internal and external surfaces. If we assume the effective density 1.6 g/cm^3 for the nanopipe walls, then the expected wall thicknesses for CMK-5 samples L, M, and S given by eq 2 will be 0.99, 0.83, and 0.74 nm, respectively. These values are in fair agreement with those presented in Table 1.

The above considerations are valid only if the carbon precursor occupies the entire pore volume of the template and if carbon is not removed from the mesopores during the process of polymerization and pyrolysis. For samples L, M, and S the pore filling was controlled by the incipient wetness procedure, and for sample LG the amount of acenaphthene was specially chosen to fill the pore volume. The adsorption analysis performed for all the samples after the precursor polymerization step revealed no mesopores, which confirmed the mesopore filling by the carbon precursor. From this, taking into account the template pore volume, the carbon precursor density, and the weight fraction of carbon in the precursor, the expected content of carbon in the silica/carbon composites should be 49 wt % for sample LG and 37 wt % on average for samples L, M, and S. This expected carbon content for the composites L, M, and S is close to that determined by TGA (Table 3), which indicates only a small loss of carbon in the process of silica/carbon composite formation using furfuryl alcohol. However, the carbon content in composite-LG is twice as lower as the expected one, indicating sufficient loss of carbon in the synthesis utilizing acenaphthene. Major loss of the precursor from sample LG was observed after the high-temperature vacuum pyrolysis. Therefore, the above volumetric estimations of the expected nanopipe wall thickness cannot be done correctly for sample LG.

Finally, we can check the obtained geometric characteristics of CMK-5 carbons and the carbon density estimations by comparing idealized carbon contents in the silica/carbon composites with those determined from TGA. As seen from Tables 1 and 3, the unit cell parameters of the carbon and the composite samples are nearly identical, which suggests that the carbon material structure was not seriously distorted after dissolving the silica template walls. Thus, we can assume that the distribution of carbon in the CMK-5 materials is close to that in the respective silica/carbon composites. From this we can derive the idealized mass ratio of carbon to silica in the composites using simple geometric considerations taking into account the volume fractions occupied by silica and carbon and their densities,

$$\frac{m(C)}{m(SiO_2)} = \frac{\rho_c}{\rho_s}\left(\frac{D_e^2 - D_i^2}{2\sqrt{3}\pi^{-1}a^2 - D_e^2} + \frac{\rho_1}{\rho_0}\right)\left(1 - \frac{\rho_1}{\rho_0}\right)^{-1} \quad (3)$$

where ρ_c and ρ_s are the densities of carbon and silica.

(29) Kruk, M.; Jaroniec, M.; Sayari, A. *Langmuir* **1997**, *13*, 6267.
(30) Jankowska, H.; Swiatkowski, A.; Choma, J. *Active Carbon*; Ellis Horwood: Chichester, UK, 1991.

From eq 3, using the value 2.2 g/cm^3 for the density of amorphous silica and our estimation 1.6 g/cm^3 for the density of carbon, the idealized contents of carbon in composites L, M, and S can be evaluated as 35, 33, and 32 wt %, respectively, which agrees perfectly with the values determined from TGA.

The values ρ_1/ρ_0 presented in Table 1 characterize the relative density of interconnections between the carbon nanpipes. Since both scattering density values ρ_1 and ρ_0 for CMK-5 correspond to carbon, their ratio can be interpreted as a fraction of volume occupied by the carbon interconnections in the space between the nanopipes. In turn, this ratio can be related to the complementary porosity of the parent SBA-15 template, namely, to the fraction of the template wall volume occupied by the complementary pores. However, the direct relation between the ratio ρ_1/ρ_0 and the template complementary porosity can only be valid if one assumes that all the complementary pores were filled by the carbon precursor and that all of them participated in the formation of the carbon interconnections. Besides, the interpretation of this ratio also depends on the assumption about zero density of matter in the nanopipe centers. The above assumptions should be independently verified, but at least the ratio ρ_1/ρ_0 can be considered as an estimate for the lower limit of the template complementary porosity. For the SBA-15 templates used in this study we may conclude that their walls were about 15% porous as a minimum, based on the values from Table 1. Ravikovitch and Neimark[28] have recently applied the NLDFT method[31,32] in the adsorption analysis of SBA-15 materials similar to Silica-L sample. They determined the total pore volume and the volume of the intrawall pores as 0.86 and 0.24 cm^3/g, respectively, from which the complementary porosity of the silica walls could be evaluated as 30%. For the SBA-15 sample calcined at 1173 K the NLDFT analysis gave the total and the intrawall pore volumes of 0.64 and 0.12 cm^3/g, respectively,[28] which corresponded to the silica wall porosity of ca. 20%. Taking into account the pyrolysis temperature 1173 K applied in our synthesis, the SBA-15 template wall porosity value 20% given by the NLDFT is in reasonable consistency with our estimation of its lower limit 15%.

The structure parameters of samples CMK-5-LG and CMK-5-L, synthesized using the same initial SBA-15 template, are found to be nearly identical (see Table 1) despite the two different carbon precursors utilized for their preparation. Using acenaphthene instead of furfuryl alcohol, one might expect obtaining thicker nanopipe walls since the weight fraction of carbon in acenaphthene is considerably higher. The absence of the expected wall thickening in CMK-5-LG can be explained by higher loss of carbon from Composite-LG during the vacuum pyrolysis as already discussed above.

As seen in Figures 1 and 4, CMK-5-LG exhibits higher and narrower XRD peaks compared to CMK-5-L, which suggests its better mesostructure ordering. Better ordering of CMK-5-LG compared to that of the remaining carbons is also reflected in the lower value of the mean amplitude of displacement (disordering) of structure elements derived from the Debye−Waller factors as listed in Table 1. Recently, a series of nanorod and nanoframework mesostructured carbons synthesized using acenaphthene as a carbon precursor was presented, which was demonstrated to exhibit greater mechanical strength, thermal stability, and graphitization degree compared to similar carbons based on furfuryl alcohol precursor.[16] In our case the superior structural ordering of CMK-5-LG can also be logically attributed to its higher mechanical strength, which protects the structure from distortions. Wide-angle XRD measurements (Figure 6) showed definite enhancement of the diffraction maxima related to the graphitic ordering for CMK-5-LG carbon compared to that for CMK-5-L. This suggests higher graphitization degree for CMK-5-LG resulted from the use of the aromatic carbon precursor, though the nanopipe walls in the carbons studied are too thin to be appreciably graphitic. As seen from Table 1, the pore volume and the surface area of CMK-5-LG are somewhat smaller than those of the remaining samples. Since the structure parameters of samples CMK-5-LG and CMK-5-L determined from XRD modeling are basically the same, the most realistic explanation of this distinction of CMK-5-LG sorption characteristics may be its lower microporosity, which is typical of carbons obtained from polyaromatic precursors.

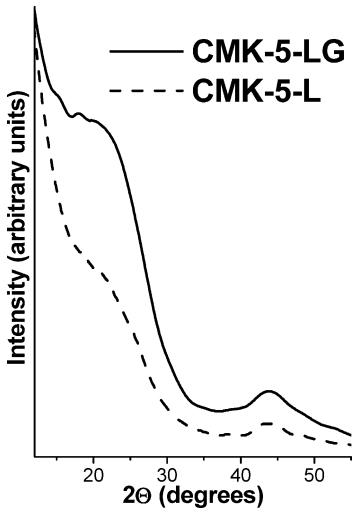

Figure 6. X-ray diffractograms of the mesostructured carbons synthesized using acenaphthene (CMK-5-LG) and furfuryl alcohol (CMK-5-L).

From the above considerations we may deduce the main factors governing the formation of carbon nanopipes in CMK-5 materials synthesized using furfuryl alcohol and acenaphthene as carbon precursors. The nanopipe formation in the process of the high-temperature vacuum pyrolysis of the polymerized furfuryl alcohol is mainly due to the volume shrinkage of the carbon precursor without its removal from the template. The strong interaction of furfuryl alcohol precursor with silica template walls facilitates the nanopipe formation. In the case of acenaphthene, its interaction with the template is weaker and the essential loss of the carbon precursor during the pyrolysis greatly influences the formation process and the final structure characteristics of the carbon nanopipes.

(31) Ravikovitch, P. I.; Haller, G. L.; Neimark, A. V. *Adv. Colloid Interface Sci.* **1998**, *77*, 203.
(32) Ravikovitch, P. I.; O'Domhnaill, S. C.; Neimark, A. V.; Schuth, F.; Unger, K. K. *Langmuir* **1995**, *11*, 4765.

4. Conclusions

The combined use of TEM image analysis and XRD structure modeling allowed detailed and comprehensive structural characterization of a series of ordered carbon nanopipe materials CMK-5 synthesized using three different mesoporous SBA-15 templates and two carbon precursors. The materials present highly ordered 2-D hexagonal arrays of carbon nanopipes. The carbon nanopipe shape was characterized by both TEM and XRD modeling as being cylindrical without detectable hexagonality. The nanopipes are interconnected by carbon matter formed inside the complementary pores of the template walls. The interconnections are distributed uniformly between the nanopipe external surfaces. The degree of the material interconnectivity, which is given by the volume fraction occupied by the carbon interconnections between the nanopipes, was determined to be around 15%. Both the nanopipe diameter and the wall thickness decrease with decreasing the template pore width, which correlates with the synthesis procedure. The nanopipe wall thickness was determined to range from 1.1 to 0.7 nm depending on the template applied. The averaged effective nanopipe wall density of the materials synthesized using furfuryl alcohol was estimated as 1.6 g/cm^3, which is noticeably lower than the absolute density of amorphous carbon ($\sim$2 g/cm^3) and indicative of the wall roughness and microporosity. The carbon yield in the process of the materials preparation utilizing furfuryl alcohol was found to be better than 84% of the total carbon atoms, owing to strong interaction of this precursor with the silica template. The carbon yield in the acenaphthene-based synthesis was lower, which was reflected in the final structure parameters. On the other hand, the use of acenaphthene as a carbon precursor resulted in better organized (and, presumably, rigid) material mesostructure and higher carbon graphitization.

Acknowledgment. This work was supported by the grants of INTAS 01-2283, KRSF-RFBR 02-03-97704, RFBR 03-03-32127, the Creative Research Initiative Program of the Korean Ministry of Science and Technology, and School of Molecular Science through the Brain Korea 21 project.

CM0352652